Rivers and floodplains as key components of global terrestrial water storage variability

Augusto Getirana[1,2], Sujay Kumar[1], Manuela Girotto[3,4], Matthew Rodell[1]

[1]Hydrological Sciences Laboratory, NASA Goddard Space Flight Center, Greenbelt, MD

[2]Earth System Science Interdisciplinary Center, University of Maryland, College Park, MD

[3]Global Modeling and Assimilation Office, NASA Goddard Space Flight Center, Greenbelt, Maryland, USA

[4]GESTAR, Universities Space Research Association, Columbia, Maryland, USA

Key points

1. SWS contributes to TWS primarily in the tropics, and in major rivers flowing over arid regions or at high latitudes.

2. SWS has low impact in Western U.S., Northern Africa, Middle-East and central Asia and most of Australia.

3. Rivers and floodplains store 2400km^3 with an annual variability of 2700km^3, contributing to 7% of TWS change globally.

Abstract

This study aims to quantify the contribution of rivers and floodplains on the global terrestrial water storage (TWS) variability. We use state-of-the-art models to simulate

land surface processes and river dynamics in order to separate TWS into its main components. Based on a proposed impact index, we show that surface water storage (SWS) contributes to 7% of TWS globally, but that contribution highly varies spatially. The primary contribution of SWS to TWS is in the tropics, and in major rivers flowing over arid regions or at high latitudes. About 20-23% of both Amazon and Nile basins' TWS changes are due to SWS. SWS has low impact in Western U.S., Northern Africa, Middle-East and central Asia. Based on comparisons against GRACE-based estimates, we conclude that using SWS significantly improves TWS simulations in most South America, Africa and Northern India, confirming the need for SWS as a key component of TWS change.

1. Introduction

Since the launch of the Gravity Recovery and Climate Experiment (GRACE) mission (Tapley et al., 2004) in 2002, the scientific community has gained significant insight into terrestrial water storage (TWS) variations around the world. Still, understanding of the relationship between TWS variations and changes in its individual components (groundwater, soil moisture, surface waters, snow, and vegetation water storage) has not advanced beyond small-scale studies based on in situ data (e.g., Rodell and Famiglietti, 2001). Although a few studies have demonstrated the impact that surface water storage (SWS) has on TWS in tropical basins (e.g. Papa et al., 2013; Pokhrel et al., 2013; Salameh et al., 2017), the vast majority of investigations on TWS decomposition systematically neglect SWS by assuming that its contribution to TWS is trivial (Houborg et al., 2012). Such studies have combined either model outputs or observations with GRACE data in order to estimate groundwater variability and change over the U.S.

(Famiglietti et al., 2011), India (Rodell et al., 2009; Tiwari et al., 2009; Chen et al., 2014; Joodaki et al., 2014; Girotto et al., 2017) and the Middle East (Voss et al., 2013). The contribution of reservoir operation to global TWS change has also been evaluated in Zhou et al. (2016), but neglecting the contribution of rivers and floodplains. Among the GRACE data assimilation (DA) initiatives, very few studies have considered SWS, mostly using relatively simple water balance models and approaches (Eicker, et al., 2014; Van Dijk et al., 2014; Tian et al., 2017). However, the majority assumes TWS as the sum of land surface model (LSM) water storage (LWS) components, e.g. groundwater storage (GWS), soil moisture (SM), snow water equivalent (SWE) and total canopy interception water storage (CAN) (e.g. Zaitchik et al., 2008; Kumar et al., 2016; Girotto et al., 2016, 2017). Notably these studies ignore the SWS contribution from rivers, floodplains, wetlands, lakes and reservoirs. Even though that assumption might be a close representation of the truth in specific locations, as evidenced in Rodell & Famiglietti (2001) over Illinois, in the U.S., the actual impact of SWS on the global TWS change and its spatial variability is unknown.

Based on the aforementioned limitations in the TWS representation and a current lack of knowledge on the actual weight of SWS on global TWS and its spatial variability, the objective of this study is to determine the actual impact of SWS on TWS change within a modeling framework. Two state-of-the-art models, the Noah LSM with multiparameterization options (Noah-MP: Niu et al., 2011) and the Hydrological Modeling and Analysis Platform (HyMAP) river routing scheme (Getirana et al., 2012), are combined in order to represent the physical processes controlling the global water balance and dynamics. An impact index is proposed and applied globally, allowing the

identification of how different water storage components contribute to TWS variability. We further investigate the spatially distributed gain in accuracy obtained by summing SWS and LWS, as compared with GRACE-based TWS estimates. An inherent assumption of the study is that Noah-MP and HyMAP provide realistic and compatible estimates of variations in the TWS components. We believe this is reasonable based recently published evaluations (e.g. Xia et al., 2017; Getirana et al., 2017), however, it will lead to uncertainty in our results. Further, the fact that these models do not account for human impacts on the water cycle, including irrigated agriculture and reservoir operations, is a limitation. Evaluation of uncertainties related to inaccurate model parameterization, limited representation of physical and anthropogenic processes, and forcing errors is beyond the scope of this work.

2. Modeling framework and evaluation

The model run was performed within the NASA Land Information System (LIS: Kumar et al., 2006), where Noah-MP and HyMAP are one-way coupled. This means that, at each time step, gridded surface runoff and baseflow simulated by Noah-MP are transferred to HyMAP and used to simulate spatially continuous surface water dynamics. No information is returned from HyMAP to Noah-MP.

The Noah-MP land surface model

The Noah-MP LSM, which is jointly developed and maintained by the National Center for Atmospheric Research (NCAR) and the National Centers for Environmental Prediction (NCEP), is a multi-physics version of the community Noah LSM. Similar to traditional LSMs, Noah-MP maintains surface energy and water balances while

simulating direct evaporation from soil, transpiration from vegetation, evaporation of interception and snow sublimation, and estimating key surface energy and moisture prognostics such as land surface temperature, snowpack, soil moisture and soil temperature. In addition, Noah-MP incorporates extensive physics upgrades over the original Noah including the representation of dynamic vegetation phenology, a carbon budget and carbon-based photosynthesis, an explicit vegetation canopy layer, a three-layer snow physics component, and a groundwater module with a prognostic water table (Niu et al., 2011).

HyMAP river routing scheme

HyMAP is a global scale river routing scheme capable of simulating flow dynamics in both rivers and floodplains. In this study, HyMAP was utilized with the local inertia formulation (Bates et al., 2010; Getirana et al., 2017), accounting for a more stable and computationally efficient representation of backwater effects. SWS [mm] is obtained by dividing the water stored in rivers and floodplains by the grid cell surface area.

Evaporation from open waters is considered in HyMAP, resulting in an improved representation of the water budget over wet surfaces, not represented in Noah-MP. That is possible because the physical relationship between the water surface and atmosphere has been simplified, such as considering the air and surface water temperatures approximately the same. The Penman–Monteith formula is used in this context. Ocean tides have been neglected in this study. Thus, the downstream boundary water elevation near river outlets is set to zero meters constant over time. More details on the HyMAP parameterization can be found in Getirana et al. (2012, 2013).

111 Although lakes and reservoirs have an important role in the water storage and dynamics
112 at the regional and global scales (e.g. Haddeland et al., 2006; Doll et al., 2009), they are
113 currently not featured in HyMAP. As a consequence, they have been neglected in this
114 study. In this sense, SWS is exclusively represented by water stored in rivers and
115 floodplains. This means that the amplitude and timing of simulated water storage
116 components in regions highly impacted by human activities, such as the U.S., parts of
117 Western Europe, and Southern and Eastern Asia, might considerably differ from reality.

118 **Modeling configuration**

119 The Princeton meteorological dataset is used as forcing for Noah-MP. The dataset is
120 available on a 3-hourly time step and at a 1-degree spatial resolution (Sheffield et al.
121 2006) for the 1948–2014 period. LIS/Noah-MP/HyMAP was run for 35 years (1980-
122 2014) at 1-hour time step and 1-degree spatial resolution. The Courant–Freidrichs–Levy
123 (CFL) condition is used in order to determine HyMAP's optimal time steps for numerical
124 stability (Bates et al., 2010; Getirana et al., 2017). A 32-year spinup was performed
125 allowing the models' water storage components to reach stability.

126 **Evaluation procedure**

127 Two evaluation procedures have been performed in order to determine the impact SWS
128 on TWS: first, an impact index *I* has been defined here as a function of each water
129 storage component contribution *C* to TWS. And *C* is defined as the sum of absolute
130 monthly climatological anomaly values:

131 $$C_i = \sum_{t=1}^{12} \left| S_{i,t} - \bar{S}_i \right| \quad (1)$$

$$I_i = \frac{C_i}{\sum_{i=1}^{nc} C_i} \quad (2)$$

where *i* and *t* are indexes related to water storage components and time step, respectively, and *nc*=5, corresponding to the water stored (*S*) in the components considered in this study: SWS, GWS, SM, SWE and CAN. The sum of impact indexes of all water storage components equals 1.

Such an index is preferred over the ratio of amplitudes, as suggested in previous studies (e.g. Pokhrel et al., 2013) due to the fact that occasional lags between the different water storage components may result in impact values superior to the unit. Using the proposed index guarantees that the sum of all I_i equals to one. The impact evaluation has been performed for the full simulation period, i.e. from 1980 to 2014.

Impacts are evaluated globally and at the basin scale. In that sense, we selected the 15 largest river basins, plus Ganges-Brahmaputra, Mekong and Tigris-Euphrates River basins. Table 1 summarizes the selected river basins and lists 17 gauge stations used to evaluate streamflow simulations through long-term averages. Streamflow observations are available through the Global Runoff Data Centre (GRDC) at the daily time step (except for the monthly observations at El Ekhsase, in the Nile River). Stations draining the largest surface have been chosen for all selected basins, except for the Indus and Tigris-Euphrates Rivers, where no data is available for the study period.

The second evaluation quantifies the gain in considering SWS as part of TWS by comparing simulated LWS and TWS (i.e. SWS+LWS) against GRACE-based TWS using the Kling-Gupta (KG) efficiency coefficient (Gupta et al., 2009). KG measures the Euclidean distance from an ideal point of the Pareto line and is a function of the

correlation (r), bias (β) and standard deviation ratio (γ), also called variability, between simulations (s) and observations (o):

$$KG = 1 - \sqrt{(r-1)^2 + (\beta-1)^2 + (\gamma-1)^2} \quad (3)$$

$$\beta = \frac{\mu_s}{\mu_o} \quad (4)$$

$$\gamma = \frac{\sigma_s}{\sigma_o} \quad (5)$$

where μ and σ stand for the mean and standard deviation of TWS time series. The optimal value for r, β, γ and KG is 1. Since the KG is computed for anomaly time series, the bias term is neglected. This means that KG is a function of phasing and amplitude ratio between s and o. The spatial distribution of improvements and deterioration with the inclusion of SWS is obtained with the differential KG (i.e. $\Delta KG = KG_{TWS} - KG_{LWS}$).

The version RL05 spherical harmonics fields (Landerer and Swenson, 2012) of GRACE monthly mass grids produced by the University of Texas Center for Space Research (CSR) are used in this study. These data are the truncated and smoothed using a Gaussian filter and are provided on a 1-degree global grid at a monthly time step. The TWS comparison has been performed for the 2003-2014 period, when both meteorological forcings and GRACE data overlap.

Monthly SWS and LWS simulations were also smoothed using a 300 km half-width Gaussian filter, then re-gridded onto the GRACE grid. These operations were needed in order to obtain simulations that were spatially and temporally consistent with the GRACE-based TWS fields. Details on the smoothening process can be found in Wahr et

al. (1998). It is important to note that this procedure was only performed for the comparison against GRACE data.

3. Results and Discussion

Impacts on the terrestrial water storage change

Results indicate that all land surface on Earth (~112×10^6 km^2, Greenland excluded) stores about 2400km^3 of water in rivers and floodplains. This number is in the same order of magnitude as previous estimates found in the literature, varying from 2000km^3 (Oki and Kanae, 2006) to 2120km^3 (Shiklomanov, 1993). 30% of that water (or ~720km^3) is concentrated in the Amazon basin (see Table 1 for mean SWS values at the selected 18 river basins). Globally, I_{SWS} is 7%, compared to 15%, 55% and 23% from I_{GWS}, I_{SM} and I_{SWE}. However, these impacts have a high spatial variability. Fig. 1 shows the impact index spatial distribution of the four water storage components (SWS, GWS, SM and SWE - canopy interception CAN was neglected in the analysis due its minimal impact). I_{SWS} can be seen in tropical areas in South America, Africa and Asia, and along most major global rivers. I_{SWS} is particularly high along rivers crossing arid regions, such as the Tigris-Euphrates (T-E) Rivers, in Iraq, the Nile and Niger Rivers over the Sahara, the Sao Francisco River, in Northeastern Brazil, among others. I_{SWS} values are also prominent over large rivers in the high latitudes, such as Ob, Yenisei, Lena, Amur, Volga and Mackenzie Rivers. Little impact has been detected over arid regions, such as the Atacama Desert, most of Northern and Eastern Africa, the Middle East, central Asia, and most of Australia. I_{SWS} values are also low over the dry Western and Mid-Western U.S. On the other hand, the SWS presents a high impact on TWS over the more humid Eastern U.S., in particular near the lower Mississippi River. Over Northern India, including the

197 Indus and Ganges-Brahmaputra (G-B) River basins, I_{SWS} values are as high as 60%. I_{SM} is
198 particularly dominant in drier regions, and also where I_{SWS} and I_{SWE} are low,
199 counterbalancing I_{GWS}, with higher values over humid areas. I_{SWE} prevails in the high
200 latitudes (mostly in the Northern Hemisphere) and the Himalayas.

201 SWS and GWS changes are in phase and have similar magnitudes in most major basins,
202 as shown in Fig. 2. This may be attributed to the fact that surface water and groundwater
203 are tightly coupled, with surface waters occurring largely where the water table intersects
204 the land surface, such that groundwater and surface water are sometimes considered to be
205 a single resource (e.g., Winter, 1998; Rodell et al., 2007). SM dominates the monthly
206 TWS change in all basins located in low latitudes, with impacts varying from 50% in the
207 Amazon to 82% in the T-E River basin. For the high latitude basins, SWE controls more
208 than 50% of TWS change, as observed in the Ob, Yenisei, Lena Volga and Mackenzie
209 River basins. In those basins, a 3-month lag is noticed between SWE and SWS, and, in
210 some cases, the amplitude of annual SWE variability is higher than TWS annual
211 variability.

212 The Amazon basin has the highest mean I_{SWS} value (27%), with a mean annual amplitude
213 of ~116mm, corresponding to 37% of the TWS' amplitude (312mm). This amplitude
214 ratio is about the mean of two estimates (27% and 50%) previously suggested in Pokhrel
215 et al. (2013) and Papa et al. (2013) using modeling and satellite data, respectively. I_{SWS} is
216 also high in the Nile basin (20%), which is due to the low GWS and SM variability in the
217 arid part of the basin. These two basins are the only ones where I_{SWS} is higher than I_{GWS}.
218 Other basins, such as Congo, Parana, Niger, Yangtze, Volga, Zambezi Indus, G-B and
219 Mekong have major SWS impacts on TWS. In particular, I_{SWS} is 13% over G-B an

220 SWS/TWS amplitude ratio of 24%, which is about half of the estimated value (50%)
221 suggested in a previous study combining multi-satellite data (Salameh et al., 2017).

222 **Comparison against GRACE data**

223 The impact of incorporating SWS in TWS is quantified using the changes in the KG
224 metric (ΔKG). The global averaged improvement of adding SWS and LWS towards a
225 better representation of TWS, compared to simply using LWS, is nominal (i.e. ΔKG=0
226 for all land surface). However, the impact of I_{SWS} in certain regions, as described in the
227 previous section, is noticeable in the ΔKG spatial distribution. The top panel of Fig. 3
228 shows the ΔKG map, highlighting 12 regions selected for further discussion, and
229 differential values of its two components, as defined in Eq. (3): differential correlation Δr
230 and differential standard deviation ratio $\Delta\gamma$. 57% of land surfaces presented improved
231 correlations with the addition of SWS, while 87% showed improved standard deviation
232 ratios. However, these improvements were small in most places, counterbalancing with
233 the high local deteriorations, and resulting in no changes in the global Δr *and* $\Delta\gamma$
234 averages.

235 The bottom panel of Fig. 3 shows the respective annual variability of GRACE
236 observations and simulated TWS, LWS and SWS. The impact of SWS is substantial over
237 South America and Africa, in particular in (1) the central Amazon, (2) the central and
238 lower Nile, (3) the Zambezi and Southern Congo River basins, and most of the Sahel.
239 SWS variability is also conspicuous in (4) Northern India and G-B River basin, (5) the
240 lower T-E River basin, and some regions in high latitudes.

241 SWS and LWS are in phase over region 1, but the large SWS annual variability increases
242 the amplitude of simulated TWS towards a better match with GRACE-based
243 observations, and significantly improves KG values. Region 2 is within the desert, where
244 LWS change is negligible; hence TWS change is governed by SWS. This can be clearly
245 observed in the annual variability shown in Fig. 3. Streamflow simulations in the Nile
246 River are overestimated in about three times (as shown in Table 1) and may be resulting
247 in higher TWS amplitudes when compared to GRACE-based observations. The Nile
248 River is also highly impacted by intense irrigation along the river and reservoir operation
249 at the Aswan dam, which can also explain differences between simulated and observed
250 TWS amplitudes. TWS change over region 3 is dominated by soil moisture and,
251 secondarily, by GWS but it experiences a non-negligible amplitude increase and a slight
252 shift in the lag with the inclusion of SWS.

253 Fig. 3 also highlights seven regions where adding SWS to LWS deteriorated the
254 comparison between TWS and GRACE. Most of those regions have in common a high
255 SWS annual variability, which significantly increases the TWS amplitude, resulting in
256 negative $\Delta\gamma$ and ΔKG. This is the case in the lower Mississippi and Yangtze River basins
257 (regions 6 and 7, respectively), as well as the Parana River basin (8), Niger's inner delta
258 (9), the lower Congo and Amur River basins (regions 10 and 11, respectively). The
259 exception is the high latitude region (12), where the considerably lagged SWS
260 counterbalances LWS, decreasing the amplitude and shifting the peaks.

261 Adding SWS to LWS improves the phase agreement between simulated TWS and
262 GRACE-based observations in regions 6, 7 and 12. Region 8 is highly impacted by
263 human activities, in particular reservoir operation (Getirana, 2016), with major dams

modifying the hydrological regime of the main river and tributaries. The Pantanal wetland, identified in the map as the upper red spot within the region, is a complex hydrological system commonly misrepresented in global-scale models. The absence of a proper representation of these natural and anthropogenic processes highly impacts the lower Parana River dynamics, resulting in an early and amplified SWS peak, negatively altering TWS simulations.

Most major river's outlets reveal a high SWS amplitude, such as observed in regions 6-11, and elsewhere in the map in Fig. 3, resulting in substantially low $\Delta\gamma$ and ΔKG values. This could be explained by HyMAP limitations in representing the surface water dynamics at the interface between rivers and oceans and major lakes.

4. Summary

The main goal of this study is to quantify the contribution of surface water storage to the global terrestrial water storage. It has been motivated by the fact that most hydrological studies employ the LSM-based water storage as TWS, neglecting SWS. Here, we use the state-of-the-art Noah-MP LSM and HyMAP river routing scheme in order to simulate the global water balance. We also propose an index to determine the impact of the major water storage components, i.e. SWS, groundwater storage, soil moisture and snow water equivalent, on TWS change. These impacts are evaluated both distributed spatially and averaged for 18 major river basins. A second analysis focuses on how adding SWS to LWS contributes to accurately estimating TWS, using GRACE-based TWS estimates as reference. The Kling-Gupta efficiency coefficient is used to determine where improvements and deteriorations happened.

286 Results show high SWS impact in the tropics, and major rivers flowing over arid regions
287 and high latitudes. We also demonstrate considerable SWS impacts in the Tigris-
288 Euphrates River basin and Northern India (including the G-B and Indus River basins),
289 where that storage component has been neglected in previous hydrological studies. In
290 addition, we show that neglecting SWS in a TWS data assimilation framework over the
291 U.S. could be an acceptable simplification for part of the country (in particular, the
292 Western and Mid-Western regions), but surface water has a significant impact in the
293 Eastern part of the country.

294 Recent developments on land surface and river dynamic modeling have resulted in major
295 improvements in the representation of large-scale hydrological processes. However, we
296 acknowledge that computational models, including those used in this study, still present
297 limitations in global parameterizations. Besides, although human activities, such as
298 reservoir operation and irrigation, have been neglected in this study, we recognize that
299 they may have non-negligible impacts on TWS change. Results may largely vary as a
300 function of different modeling configurations, so we caution that the findings presented
301 in this study are representative for adopted particular modeling system, its
302 parameterization and forcings. Further investigation considering different modeling and
303 observational techniques is highly encouraged. The coarse spatial resolution of GRACE
304 also plays an important role in the evaluation, since signals over rivers can be smoothed
305 out and may not be realistic.

306 Simplifications aside, these results will be valuable for future studies to determine the
307 importance of (i) integrating river routing schemes into LSMs, (ii) considering SWS
308 when composing or decomposing TWS, and (iii) assimilating TWS and new variables

within a multivariate DA framework in hydrology (e.g. Tian et al., 2017), based on the impact of each water storage component. In that sense, simultaneously assimilating TWS and surface water level from existing (e.g. Jason-3, SARAL/AltiKa, and Sentinel-3) and future (Surface Water and Ocean Topography - SWOT) sensors within integrated global-scale modeling systems will greatly improve our understanding the spatial and temporal variability of terrestrial water storage and its components.

Acknowledgements

This study was funded by the NASA Applied Sciences - Water Resources and NASA SERVIR Programs. GRACE land data (available at http://grace.jpl.nasa.gov) processing algorithms were provided by Sean Swenson and supported by the NASA MEaSUREs Program. Streamflow observations are available through the Global Runoff Data Centre (GRDC). Meteorological forcings are available through Princeton's Terrestrial Hydrology Group (http://hydrology.princeton.edu/data.pgf.php).

References

Bates, P. D., M. S. Horritt, and T. J. Fewtrell (2010), A simple inertial formulation of the shallow water equations for efficient two-dimensional flood inundation modeling, J. Hydrol., 387, 33–45, doi:10.1016/j.jhydrol.2010.03.027.

Doll, P., Fiedler, K., Zhang, J., 2009. Global-scale analysis of river flow alterations due to water withdrawals and reservoirs. Hydrol. Earth Syst. Sci., 13, 2413–2432.

Chen, J., Li, J Zhang, Z., Ni, S., 2014. Long-term groundwater variations in Northwest India from satellite gravity measurements. Global and Planetary Change 116 (2014) 130–138. 10.1016/j.gloplacha.2014.02.007

Eicker, A., Schumacher, M., Kusche, J., Doll, P., Schmied, H.M., 2014. Calibration/Data Assimilation Approach for Integrating GRACE Data into the WaterGAP Global Hydrology Model (WGHM) Using an Ensemble Kalman Filter: First Results. Surv Geophys. 35:1285–1309 DOI 10.1007/s10712-014-9309-8

Famiglietti, J. S., M. Lo, S. L. Ho, J. Bethune, K. J. Anderson, T. H. Syed, S. C. Swenson, C. R. de Linage, and M. Rodell (2011), Satellites measure recent rates of groundwater depletion in California's Central Valley, Geophys. Res. Lett., 38, L03403, doi:10.1029/2010GL046442.

Getirana, A., 2016. Extreme water deficit in Brazil detected from space. Journal of Hydrometeorology, 17, 591-599. DOI: 10.1175/JHM-D-15-0096.1.

Getirana, A. Boone, D. Yamazaki, B. Decharme, F. Papa, and N. Mognard, 2012: The Hydrological Modeling and Analysis Platform (HyMAP): Evaluation in the Amazon basin. J. Hydrometeor., 13, 1641–1665, doi:10.1175/JHM-D-12-021.1.

Getirana, A., Boone, A., Yamazaki, D., Mognard, N., 2013. Automatic parameterization of a flow routing scheme driven by radar altimetry data: Evaluation in the Amazon basin. Water Resources Research. DOI: 10.1002/wrcr.20077.

Getirana, A., Peters-Lidard, C., Rodell, M., Bates, P.D., 2017. Trade-off between cost and accuracy in large-scale surface water dynamic modeling. Water Resources Research. DOI: 10.1002/2017WR020519

Girotto, M., G. J. M. De Lannoy, R. H. Reichle, and M. Rodell (2016), Assimilation of gridded terrestrial water storage observations from GRACE into a land surface model, Water Resour. Res., 52, 4164–4183, doi:10.1002/2015WR018417.

Girotto, M., G. J. M. De Lannoy, R. H. Reichle, M. Rodell, C. Draper, S. N. Bhanja, and A. Mukherjee (2017), Benefits and pitfalls of GRACE data assimilation: A case

355 study of terrestrial water storage depletion in India, Geophys. Res. Lett., 44,
356 4107–4115. doi:10.1002/2017GL072994.
357 Gupta, H.V., Kling, H., Yilmaz, K.K., Martinez, G.F., 2009. Decomposition of the mean
358 squared error and NSE performance criteria: implications for improving
359 hydrological modelling. J. Hydrol. 377, 80–91.
360 Haddeland, I., T. Skaugen, and D. P. Lettenmaier, 2006: Anthropogenic impacts on
361 continental surface water fluxes. Geophys. Res. Lett., 33
362 Houborg, R., M. Rodell, B. Li, R. Reichle, and B. F. Zaitchik (2012), Drought indicators
363 based on model-assimilated Gravity Recovery and Climate Experiment (GRACE)
364 terrestrial water storage observations, Water Resour. Res., 48, W07525,
365 doi:10.1029/ 2011WR011291.
366 Joodaki, G., J. Wahr, and S. Swenson (2014), Estimating the human contribution to
367 groundwater depletion in the Middle East, from GRACE data, land surface
368 models, and well observations, Water Resour. Res., 50, 2679–2692, doi:10.1002/
369 2013WR014633.
370 Kumar, S.V., C.D. Peters-Lidard, Y. Tian, J. Geiger, P. R. Houser, S. Olden, L. Lighty, J.
371 L. Eastman, P. Dirmeyer, B. Doty, J. Adams, E. F. Wood, and J. Sheffield, 2006:
372 LIS – An interoperable framework for high resolution land surface modeling,
373 Environ. Modell. Software, 21, 1402-1415.
374 Kumar, S.V., Zaitchik, B.F., Peters-Lidard, C.D., Rodell, M., Reichle, R., Li, B., Jasinski,
375 M., Mocko, D., Getirana, A., De Lannoy, G., Cosh, M., Hain, C.R., Anderson,
376 M., Arsenault, K.R., Xia, Y., Ek., M., 2016. Assimilation of gridded GRACE
377 terrestrial water storage estimates in the North American Land Data Assimilation
378 System. Journal of Hydrometeorology. DOI: 10.1175/JHM-D-15-0157.1.

379 Landerer, F.W., Swenson, S.C., 2012. Accuracy of scaled GRACE terrestrial water
380 storage estimates. Water Resour. Res., 48, doi:10.1029/2011WR011453.
381 Niu, G.-Y., Z.-L. Yang, K. E. Mitchell, F. Chen, M. B. Ek, M. Barlage, L. Longuevergne,
382 A. Kumar, K. Manning, D. Niyogi, E. Rosero, M. Tewari, and Y. Xia (2011), The
383 community Noah land surface model with multiparameterization options (Noah-
384 MP): 1. Model description and evaluation with local-scale measurements, J.
385 Geophys. Res., doi:10.1029/2010JD015139.
386 Oki, T., Kanae, S., 2006. Global hydrological cycles and world water resources. Science,
387 313, 1068-1072.
388 Papa, F., Frappart, F., Güntner, A., Prigent, C., Aires, F., Getirana, A.C.V., Maurer R.,
389 2013. Surface freshwater storage and variability in the Amazon basin from multi-
390 satellite observations, 1993–2007, J. Geophys. Res. Atmos., 118, 11,951–11,965,
391 doi:10.1002/2013JD020500.
392 Pokhrel, Y. N., Y. Fan, G. Miguez-Macho, P. J.-F. Yeh, and S.-C. Han (2013), The role
393 of groundwater in the Amazon water cycle: 3. Influence on terrestrial water
394 storage computations and comparison with GRACE, J. Geophys. Res. Atmos.,
395 118, 3233–3244, doi:10.1002/jgrd.50335.
396 Rodell, M., Famiglietti, J. S., 2001. An analysis of terrestrial water storage variations in
397 Illinois with implications for the Gravity Recovery and Climate Experiment
398 (GRACE). Wat. Resour. Res. 37, 1327–1340.
399 Rodell, M., J. Chen, H. Kato, J. S. Famiglietti, J. Nigro, and C. R. Wilson, Estimating
400 ground water storage changes in the Mississippi River basin (USA) using
401 GRACE, Hydrogeology Journal, 15, 159-166, doi:10.1007/s10040-006-0103-7,
402 2007.

Rodell, M., Velicogna, I., Famiglietti, J.S., 2009. Satellite-based estimates of groundwater depletion in India. Nature 460, 999-1002. doi:10.1038/nature08238

Salameh, E., Frappart, F., Papa, F., Güntner, A., Venugopal, V., Getirana, A., Prigent, C., Aires, F., Labat, D., Laignel, B., 2017. 15 years (1993-2007) of surface freshwater storage variability in the Ganges-Brahmaputra River basin using multi-satellite observations. Water, 9(4), 245. DOI:10.3390/w9040245.

Sheffield, J., G. Goteti, and E. F. Wood, 2006: Development of a 50-year high-resolution global dataset of meteorological forcings for land surface modeling. J. Climate, 19, 3088–3111, doi:10.1175/JCLI3790.1.

Shiclomanov, I.A., 1996. World fresh water resources. In: Water in Crisis: A Guide to the World's Fresh Water Resources. P.H. Gleick, Ed. Oxford University Press, New York, NY, pp. 13-24

Tapley, B., S. Bettadpur, J. C. Reis, P. F. Thompson, and M. M. Watkins (2004), GRACE measurements of mass variability in the earth system, Science, 305(5683), 503–505, doi:10.1126/science.1099192.

Tian, S., P. Tregoning, L. J. Renzullo, A. I. J. M. van Dijk, J. P. Walker, V. R. N. Pauwels, and S. Allgeyer (2017), Improved water balance component estimates through joint assimilation of GRACE water storage and SMOS soil moisture retrievals, Water Resour. Res., 53, 1820–1840, doi:10.1002/ 2016WR019641.

Tiwari, V. M., J. Wahr, and S. Swenson (2009), Dwindling groundwater resources in northern India, from satellite gravity observations, Geophys. Res. Lett., 36, L18401, doi:10.1029/2009GL039401.

van Dijk, A.I.J.M., Renzullo, L.J., Wada, Y., Tregoning, P., 2014. A global water cycle reanalysis (2003–2012) merging satellite gravimetry and altimetry observations

427 with a hydrological multi-model ensemble . Hydrol. Earth Syst. Sci., 18, 2955–
428 2973. doi:10.5194/hess-18-2955-2014
429 Voss, K. A., J. S. Famiglietti, M. Lo, C. de Linage, M. Rodell, and S. C. Swenson (2013),
430 Groundwater depletion in the Middle East from GRACE with implications for
431 transboundary water management in the Tigris-Euphrates-Western Iran region,
432 Water Resour. Res., 49, doi:10.1002/wrcr.20078.
433 Wahr, J., M. Molenaar, and F. Bryan, 1998: Time variability of the earth's gravity field:
434 Hydrological and oceanic effects and their possible detection using GRACE. J.
435 Geophys. Res., 103, 30 205–30 229, doi:10.1029/98JB02844
436 Winter TC, Harvey JW, Franke QL, Alley WM (1998) Ground water and surface water: a
437 single resource. USGS Circular 1139: 79 pp.
438 Xia, Y., D. Mocko, M. Huang, B. Li, M. Rodell, K. E. Mitchell, X. Cai, and M.B. Ek,
439 Comparison and assessment of three advanced land surface models in simulating
440 terrestrial water storage components over the United States, *J. Hydrometeor.,* 18,
441 625-649, DOI: 10.1175/JHM-D-16-0112.1, 2017.
442 Zaitchik, B.F., Rodell, M., Reichle, R.H., 2008. Assimilation of GRACE Terrestrial
443 Water Storage Data into a Land Surface Model: Results for the Mississippi River
444 Basin. J. Hydrometeor, 9, 535–548.
445 Zhou, T., Nijssen, B., Gao, H., Lettenmaier, D.P., 2016. The contribution of reservoirs to
446 global land surface water storage variations. Journal of Hydrometeorology,17,
447 309-325. DOI: 10.1175/JHM-D-15-0002.1

448 **Table 1. Summary of the 15 world's largest river basins, plus Ganges-Brahmaputra,**

449 **Mekong and Tigris-Euphrates. All land surface is also listed.**

Basin #	River basin	Surface area[1] [10^3km^2]	Mean SWS [km^3]	Mean SWS annual variability [km^3]	Station	Drainage area at station[2] [10^3km^2]	Longitude	Latitude	Oserved years	Q_{obs} [$m^3.s^{-1}$]	Q_{sim} [$m^3.s^{-1}$]
1	**Amazon**	5901	719.3	700.3	Óbidos	4680	-55.5	-2.0	1980-1997	165,687	145,777
2	**Congo**	3713	148.5	175.8	Kinshasa	3475	15.3	-4.3	1980-2010	38,617	55,250
3	**Mississippi**	3184	61.4	40.6	Vicksburg	2964.3	-90.9	32.3	1980-2014	18,838	18,627
4	**Nile**	3048	67.2	97.0	El Ekhsase	2900	31.3	29.7	1980-1984	1277	4875
5	**Ob**	2629	58.2	34.1	Salekhard	2950	66.5	66.6	1980-2010	12,884	9377
6	**Parana**	2621	116.1	144.3	Timbues	2346	-60.7	-32.7	1980-2014	18,161	29,532
7	**Yenisei**	2515	62.5	38.1	Igarka	2440	86.5	67.5	1980-2011	19,457	11,231
8	**Lena**	2455	54.4	24.2	Stolb	2460	126.8	72.4	1980-2002	15,737	8242
9	**Niger**	2149	44.7	97.6	Malanville	1000	3.4	11.9	1980-1995	763	1980
10	**Amur**	1969	29.6	24.7	Bogorodskoye	17900	140.5	52.5	1980-1987	11,467	9028
11	**Mackenzie**	1770	32.2	17.3	Artic Red River	16600	-133.8	67.5	1980-2014	9192	4945
12	**Yangtze**	1735	78.1	73.3	Datong	1705	117.6	30.8	2004-2004	25,012	19,224
13	**Volga**	1404	67.6	59.2	Volgograd Power Plant	1360	44.6	48.8	1980-2010	8127	8446
14	**Zambezi**	1386	28.0	59.1	Matundo-Cais	940	33.6	-16.2	1980-2004	2155	8458
15	**Indus**	1068	5.3	5.2	-	-	-	-	-	-	-
16	**Ganges-Brahmaputra**	1472	35.6	78.8	Hardinge Bridge	846	89.0	24.1	1985-1991	11,146	10,763
					Bahadurabad	636	89.7	25.2	1985-1991	23,165	13,624
17	**Mekong**	786	42.9	90.7	Stung Treng	635	106.0	13.5	1991-1994	14,456	10,410
18	**Tigris-Euphrates**	911	3.6	5.1	-	-	-	-	-	-	-
All land surface[3]		112,134	2388.3	2706.2	-	-	-	-	-	-	-

450 **[1]Based on HyMAP parameters. [2] Based on GRDC data. [3] Greenland excluded.**

Figure 1. Spatially distributed impact of surface water storage (SWS), groundwater storage (GWS), soil moisture (SM) and snow water equivalent (SWE) for the 1980-2014 period.

Figure 2. Annual variability in mm equivalent height of water of simulated TWS, SWS, GWS, SM and SWE at 18 major river basins for the 1980-2014 period. Their impacts are also provided (ordered by importance – see colors in the legend).

Figure 3. On top, the spatial distribution of efficiency coefficients between LWS and TWS using GRACE as the reference: differential Kling-Gupta (ΔKG), differential correlation (Δr) and differential standard deviation ratio (Δγ). In the bottom, the annual variability in mm equivalent height of water of GRACE observations and simulated TWS, LWS and SWS at 12 selected regions for the 2003-2014 period.

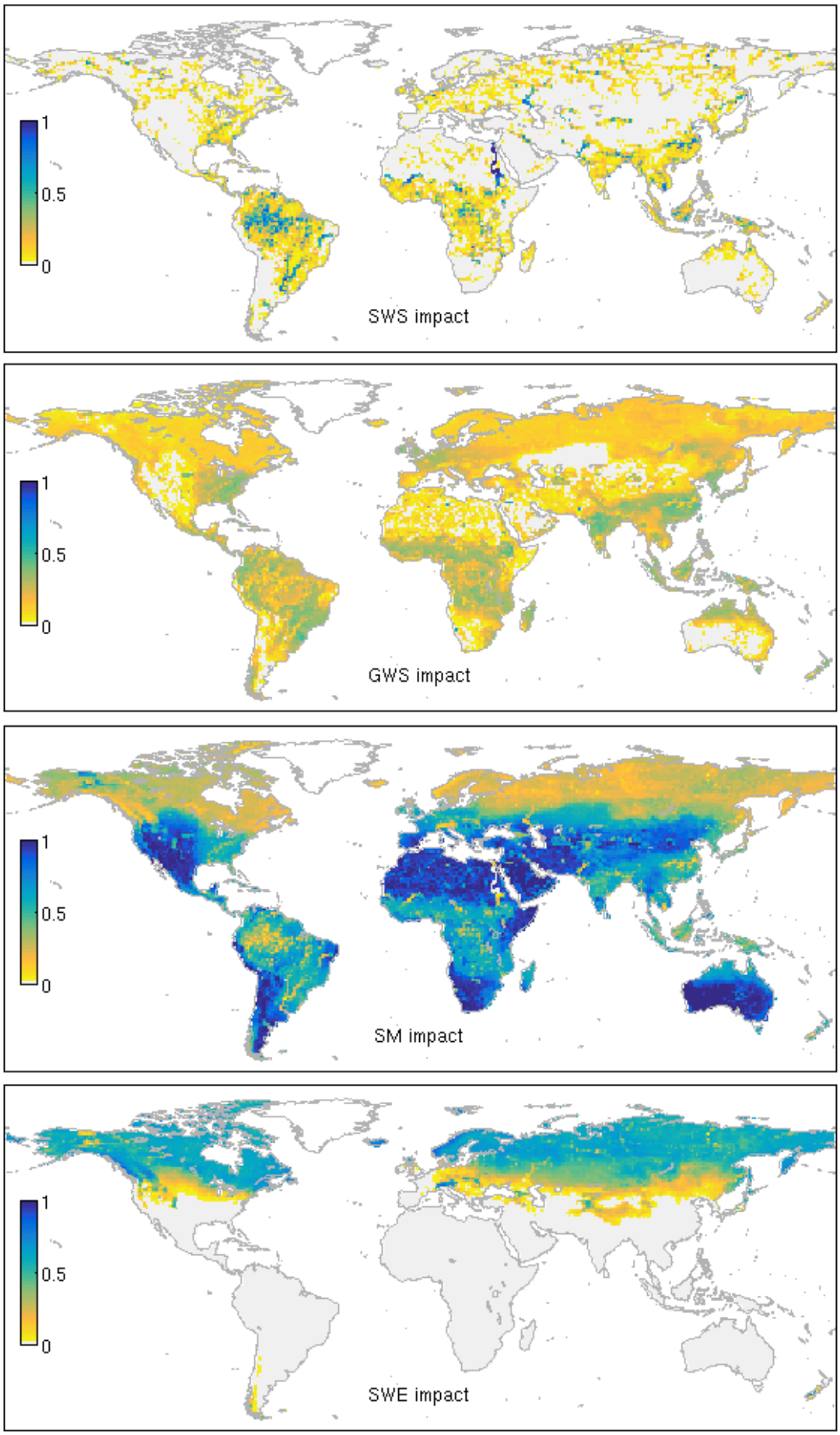
1
0.5
0
SWS impact
1
0.5
0
GWS impact
1
0.5
0
SM impact
1
0.5
0
SWE impact

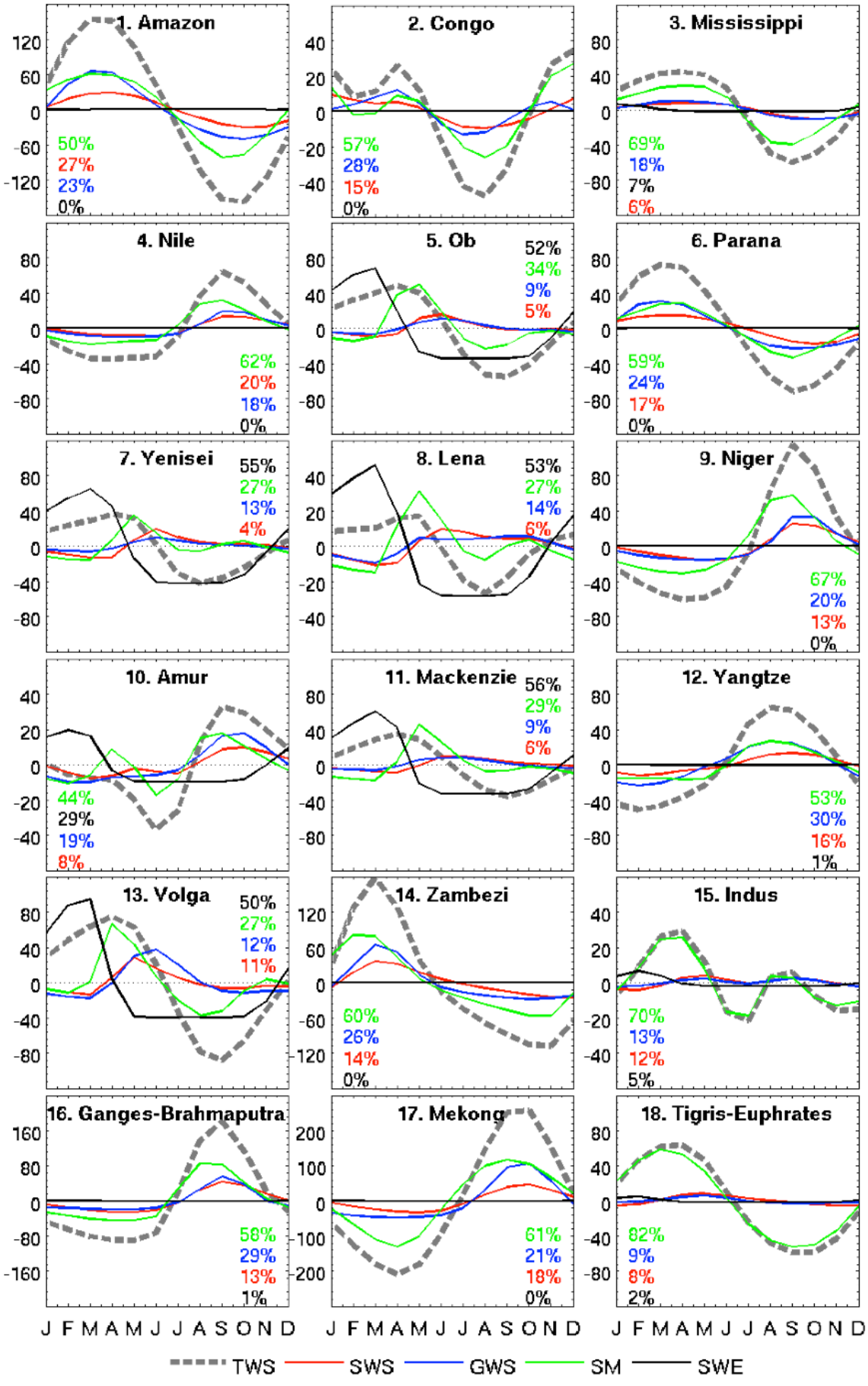
1. Amazon
50%
27%
23%
0%
2. Congo
57%
28%
15%
0%
3. Mississippi
69%
18%
7%
6%
4. Nile
62%
20%
18%
0%
5. Ob
52%
34%
9%
5%
6. Parana
59%
24%
17%
0%
7. Yenisei
55%
27%
13%
4%
8. Lena
53%
27%
14%
6%
9. Niger
67%
20%
13%
0%
10. Amur
44%
29%
19%
8%
11. Mackenzie
56%
29%
9%
6%
12. Yangtze
53%
30%
16%
1%
13. Volga
50%
27%
12%
11%
14. Zambezi
60%
26%
14%
0%
15. Indus
70%
13%
12%
5%
16. Ganges-Brahmaputra
58%
29%
13%
1%
17. Mekong
61%
21%
18%
0%
18. Tigris-Euphrates
82%
9%
8%
2%
J F M A M J J A S O N D
TWS
SWS
GWS
SM
SWE

463

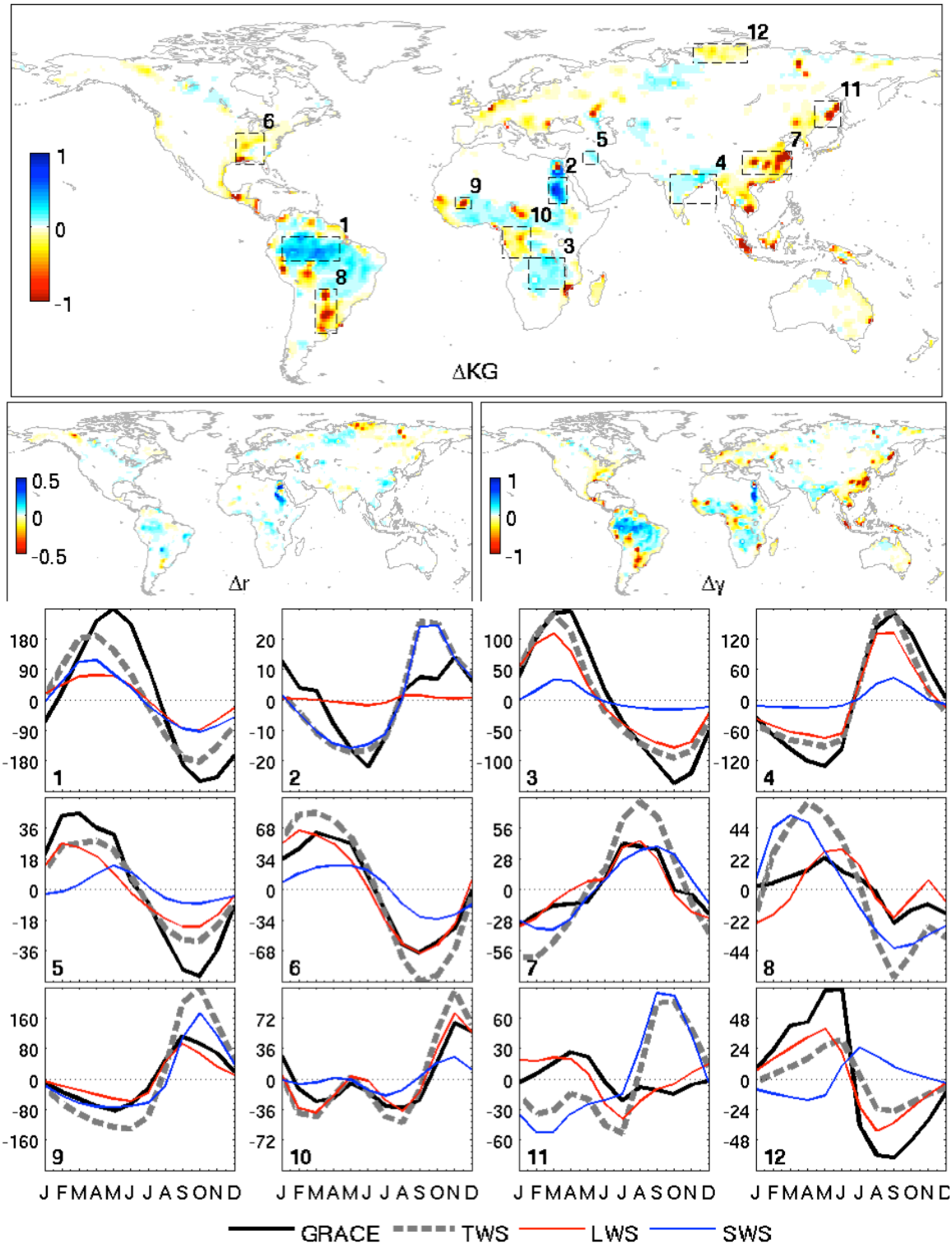
ΔKG
Δr
Δγ
GRACE
TWS
LWS
SWS
J FMAMJ J ASOND